Available online at www.sciencedirect.com

ScienceDirect

International Journal of Solids and Structures 45 (2008) 3996–4020

INTERNATIONAL JOURNAL OF SOLIDS AND STRUCTURES

www.elsevier.com/locate/ijsolstr

Closed-form structural stress and stress intensity factor solutions for spot welds under various types of loading conditions

P.-C. Lin [a], J. Pan [b,*]

[a] Department of Mechanical Engineering, National Chung Cheng University, Chia-Yi 621, Taiwan

[b] Department of Mechanical Engineering, University of Michigan, 2250 GGB Building, Ann Arbor, MI 48109-2125, USA

Received 9 August 2007; received in revised form 20 November 2007

Available online 15 February 2008

Abstract

The theoretical framework and closed-form stress intensity factor solutions in terms of the structural stresses for spot welds under various types of loading conditions are presented based on elasticity theories and fracture mechanics. A mechanics description of loading conditions for a finite plate with a rigid inclusion is first presented. The loading conditions of interest are the resultant loads on the inclusion with respect to the center of the inclusion in a finite or infinite plate and the surface tractions on the lateral surface of a finite or infinite plate. The surface tractions on the lateral surface of the plate can be decomposed into a load-balanced part and a self-balanced part. The load-balanced part is statically in equilibrium with the resultant loads acting on the inclusion. The self-balanced part can be represented by the resultant loads on the lateral surface of the plate. The resultant loads on the inclusion and the self-balanced resultant loads on the lateral surface are then decomposed into various types of symmetric and anti-symmetric parts. Based on the stress function approach and the Kirchhoff plate theory for linear elastic materials, closed-form in-plane stress, moment and transverse shear force solutions are derived for a plate with a rigid inclusion subjected to various types of resultant loads on the inclusion and various types of resultant loads on the plate lateral surface. Based on the *J* integral for a strip model, closed-form analytical stress intensity factor solutions for spot welds joining two sheets of equal thickness are derived in terms of the structural stresses around a rigid inclusion in a plate under various types of loading conditions. The closed-form solutions presented in this paper are used as the basis to develop new analytical stress intensity factor solutions for spot welds in various types of specimens presented in a subsequent paper.

Keywords: Spot weld; Fatigue; Structural stress; Stress intensity factor; *J* integral

1. Introduction

Resistance spot welding is widely used to join sheet metals in the automotive industry. These spot welds are subjected to complex multiaxial loads under service or crash conditions. The fatigue lives of spot welds in var-

* Corresponding author. Tel.: +1 734 764 9404; fax: +1 734 647 3170.
E-mail address: jwo@umich.edu (J. Pan).

0020-7683/$ - see front matter © 2008 Elsevier Ltd. All rights reserved.
doi:10.1016/j.ijsolstr.2008.02.006

ious types of specimens have been investigated by many researchers, for example, see Zhang (1999). Since a spot weld provides a natural crack or notch along the nugget circumference, fracture mechanics has been adopted to investigate the stress intensity factors at the critical locations of spot welds in order to investigate the fatigue lives of spot welds in various type of specimens (Pook, 1975, 1979; Radaj, 1989; Radaj and Zhang, 1991a,b, 1992; Sheppard, 1993; Swellam et al., 1994; Zhang, 1997, 1999, 2001; Wang et al., 2005a,b; Lin et al., 2007). The stress intensity factors usually vary point by point along the circumference of spot welds in various types of specimens. Pook (1975, 1979) gave the maximum stress intensity factors for spot welds in lap-shear specimens, coach-peel specimens, circular plates, and other bending dominant plate and beam configurations. Radaj (1989) and Radaj and Zhang (1991a,b, 1992) established the foundation to use the structural stresses to determine the stress intensity factors for spot welds under various types of loading conditions. Based on a strip model, the stress intensity factor solutions were determined in the form of the structural stress multiplied by the square root of the thickness. Sheppard (1993) used a finite element model of spot welds based on the structural stress approach to estimate the fatigue life of spot welds for lap-shear and coach-peel specimens. Swellam et al. (1994) proposed a stress index K_i by modifying their stress intensity factors to correlate their experimental results for various types of specimens. Zhang (1997, 2001) presented closed-form stress intensity factor solutions for selected critical locations of spot welds in various types of specimens based on the analytical stress solutions for a rigid inclusion in a plate under various types of loading conditions, and correlated the solutions with the experimental results of spot welds in these specimens under cyclic loading conditions. Zhang (2001) also developed a spot weld finite element model with a beam element connected by rigid spoke patterns to represent a spot weld in specimens and automotive structures. Wang et al. (2005a,b) obtained the mode I stress intensity factor solutions for spot welds in square-cup and lap-shear specimens based on their full three-dimensional finite element models. The computational solutions were compared with the analytical solution of Pook (1979) for circular-cup specimens and the new analytical solutions of Lin et al. (2007) for lap-shear specimens.

Pook (1979) indicated that for a class of transversely loaded configurations consisting of two thin plates or beams joined over part of their common plane under symmetric loading conditions, the energy release rate or the stress intensity factor at a crack tip depends on the bending moment acting to the beam or plate in the vicinity of the crack tip. Wang et al. (2005a) conducted a three-dimensional finite element analysis of circular plates with connection under opening loading conditions. The computational results indicate that the stress intensity factor along the crack front can be correlated very well with the analytical solutions based on the bending moments or the corresponding structural stresses for thin plates with connection. In this case, the circular plates with connection are subjected to axisymmetric loading conditions and the stress intensity factor along the crack front is uniform. For spot welds in lap-shear specimens, the configuration is more complex and the stress intensity factors vary along the crack front. Wang et al. (2005b) conducted a three-dimensional finite element analysis of a nearly square large lap-shear specimen. The ratio of the specimen width to the nugget diameter for the lap-shear specimen is very large so that the exact analytical solution for the infinite plate model matches the approximate analytical solution for the finite plate model (Wang et al., 2005b). The computational results indicated that the stress intensity factor at the critical locations agrees very well with the analytical solution based on the bending moments and the membrane forces or the corresponding structural stresses. For the nearly square lap-shear specimen, the stress intensity factors along the crack front are non-uniform. The results of the three-dimensional finite element analyses of Wang et al. (2005a,b) suggest that using the bending moments and the membrane forces or the corresponding structural stresses to obtain the stress intensity factors for spot welds assumed as rigid inclusions in thin plates can be quite accurate.

The closed-form solutions for thin plates with rigid inclusions under shear, central bending, counter bending, and opening loading conditions were obtained by Muskhelishvili (1953), Reißner (1929), Goland (1943), Timoshenko and Woinowsky-Krieger (1959), and Lin et al. (2007), respectively. These solutions except those of Goland (1943) and Lin et al. (2007) were used by Zhang (1997, 1999, 2001) to obtain the structural stresses at several critical locations of spot welds in various types of specimens and automotive structures, where the spot welds were treated as rigid in the analytical or numerical solution procedures. Rupp et al. (1990, 1995) used a beam element model whereas Salvini et al. (1997, 2000) and Vivio et al. (2002) used a spot weld assembly finite element model to represent a spot weld to obtain the resultant forces and moments through the spot weld for fatigue life estimations. Salvini et al. (2000) listed the analytical stress, moment, and transverse shear

force solutions for a spot weld under the resultant forces and moments through the spot weld for determination of the structural stresses around the nugget. Their analytical solutions are obtained from those for a rigid inclusion in a circular plate with clamped boundary conditions along the edge of the plate. The classical solutions of Muskhelishvili (1953), Reißner (1929), Goland (1943), Timoshenko and Woinowsky-Krieger (1959) were obtained from the complex variable approach and the Kirchhoff plate theory. In order to develop new analytical solutions for spot welds in five types of commonly used specimens in a subsequent paper (Lin and Pan, 2008a), all analytical solutions needed are derived again here using the stress function approach and the Kirchhoff plate theory. From this viewpoint, this paper can be considered as a comprehensive review paper where most of relevant closed-form analytical solutions for a plate with a rigid inclusion under various types of loading conditions are derived and presented in a consistent manner. These analytical solutions are useful for engineers to estimate the fatigue lives of spot welds under various types of loading conditions.

In this paper, we first present a detailed description of the loading conditions for a finite plate with a rigid inclusion. We emphasize the decomposition of the traction on the lateral surface of the plate. The self-balanced part of the traction has not received attention in the literature. Recently, Lin et al. (2007) obtained an approximate analytical solution for a finite plate with a rigid inclusion under self-balanced counter bending conditions in order to accurately model the computational results of the mode I stress intensity factor solutions for spot welds in lap-shear specimens. This analytical solution becomes the most critical input for the development of new stress intensity factor solutions for spot welds in various types of specimens. The analytical stress intensity factor solutions obtained by Zhang (1997, 1999, 2001) for various types of specimens were obtained from the solution for a plate with a rigid inclusion under center bending conditions substituting for the solution for a plate with a rigid inclusion under self-balanced counter bending conditions. The analytical stress intensity factor solutions of Zhang (1997, 1999, 2001) are listed for the selected critical locations of spot welds in various types of specimens. The new analytical stress intensity factor solutions of Lin and Pan (2008a), in contrast, provide detailed stress intensity factor solutions around the entire nugget circumference in various types of specimens. Most importantly, the new analytical solutions provide the size dependence of the mode I stress intensity factor solutions for spot welds in various types of specimens to allow future consolidations of the fatigue test data obtained from specimens of different designs in the literature.

For various types of laboratory specimens under cyclic loading conditions, the critical material elements of interest are usually under proportional cyclic loading conditions. Therefore, the stress intensity factor solutions for selected critical locations of spot welds are sufficient to examine the fatigue lives of spot welds in these specimens (Zhang, 1997, 1999, 2001). However, for spot welds in structural components under complex service loads, the material elements around the nugget may be subject to non-proportional cyclic loading conditions. Therefore, the stress and stress intensity factor solutions under various types of loading conditions need to be expressed in terms of the angular location along the nugget circumference in order to determine the critical locations for fatigue crack initiation. For example, Rupp et al. (1990, 1995), Salvini et al. (1997, 2000, 2007) and Vivio et al. (2002) used their spot weld finite element models to obtain the resultant forces and moments through a spot weld and then to determine the critical locations for fatigue crack initiation. It is clear that the detailed stress and stress intensity factor solutions along the nugget circumference are needed to predict the fatigue lives of spot welds under non-proportional cyclic loading conditions. It should be emphasized that the resultant forces and moments through the nugget can only be used to obtain a partial contribution of the structural stresses around the nugget circumference. In order to obtain the full structural stresses around the nugget circumference, the contributions of the self-balanced resultant loads on the lateral surface of the plate as emphasized in this paper are needed to be considered.

In this paper, the theoretical framework and closed-form stress intensity factor solutions in terms of the structural stresses for spot welds under various types of loading conditions are presented based on elasticity theories and fracture mechanics. A mechanics description of loading conditions for a finite plate with a rigid inclusion is first presented. The loading conditions of interest are the resultant loads on the inclusion with respect to the center of the inclusion in a finite or infinite plate and the surface tractions on the lateral surface of a finite or infinite plate. The surface tractions on the lateral surface of the plate can be decomposed into a load-balanced part and a self-balanced part. The load-balanced part is statically in equilibrium with the resultant loads acting on the inclusion. The self-balanced part can be represented by the resultant loads on the lateral surface of the plate. The resultant loads on the inclusion and the self-balanced resultant loads on the

lateral surface are then decomposed into various types of symmetric and anti-symmetric parts. Based on the stress function approach and the Kirchhoff plate theory for linear elastic materials, closed-form in-plane stress, moment and transverse shear force solutions are derived for a plate with a rigid inclusion subjected to various types of resultant loads on the inclusion and various types of resultant loads on the plate lateral surface. Based on the J integral for a strip model, closed-form analytical stress intensity factor solutions for spot welds joining two sheets of equal thickness are derived in terms of the structural stresses around a rigid inclusion in a plate under various types of loading conditions. The closed-form solutions presented in this paper are used as the basis to develop new analytical stress intensity factor solutions for spot welds in various types of specimens presented in a subsequent paper (Lin and Pan, 2008a).

2. A spot weld in a finite plate under general loading conditions

Fig. 1(a) schematically shows two metal sheets of equal thickness joined by a spot weld. As shown in Fig. 1(a), the surface tractions $\mathbf{T}_U$ and $\mathbf{T}_L$ are applied on the lateral surfaces of the upper and lower sheets, respectively. In this investigation, we idealize the weld nugget as a circular cylinder as shown in Fig. 1(a). Next, we consider the upper half of the weld nugget in the upper sheet as shown in Fig. 1(b) without loss of generality. Fig. 1(b) shows that the surface traction $\mathbf{T}_S$ is on the bottom surface of the upper half nugget.

Fig. 1(c) shows a Cartesian coordinate system where x and y represent the in-plane coordinates and z represents the out-of-plane coordinate. The origin of the Cartesian coordinate system is located at the center of the upper weld nugget, which is on the middle plane of the plate. As shown in Fig. 1(c), the surface traction $\mathbf{T}_S$ in Fig. 1(b) can be represented by a resultant force $\mathbf{F}$ and a resultant moment $\mathbf{M}$ acting at the origin of the Cartesian coordinate system. On the lateral surface of the upper sheet, the surface traction $\mathbf{T}_U$ in Fig. 1(b) can be decomposed into a load-balanced part $\mathbf{T}_U^{Load}$ and a self-balanced part $\mathbf{T}_U^{Self}$. Note that the load-balanced part $\mathbf{T}_U^{Load}$ is statically in equilibrium with the resultant loads $\mathbf{F}$ and $\mathbf{M}$. The self-balanced part $\mathbf{T}_U^{Self}$ satisfies self-equilibrium and has no contribution to the resultant loads $\mathbf{F}$ and $\mathbf{M}$.

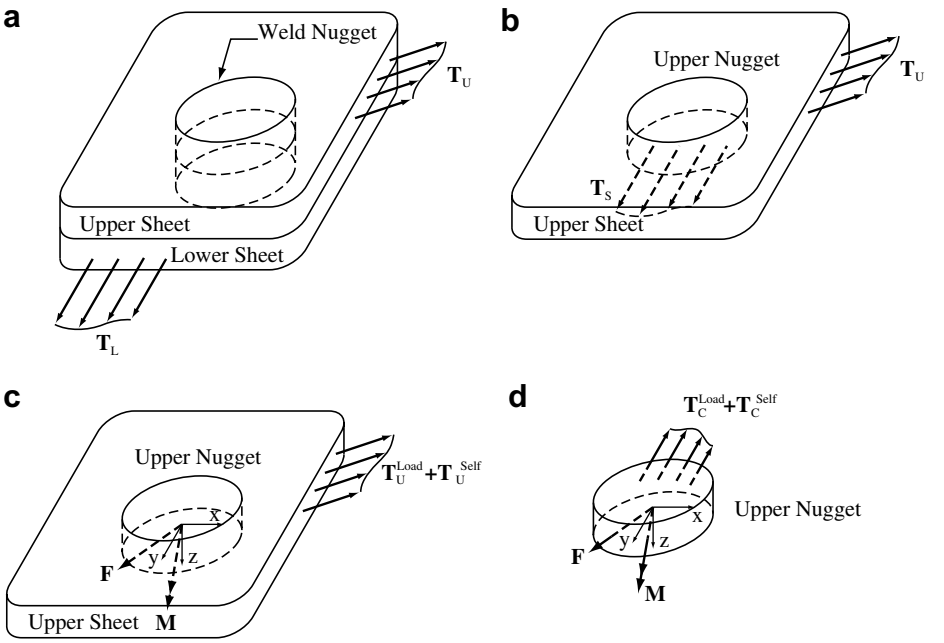

Fig. 1. (a) Two metal sheets are joined by a spot weld. The metal sheets are under surface traction $\mathbf{T}_U$ and $\mathbf{T}_L$. (b) The upper sheet with the upper half nugget. The upper sheet is under the surface tractions $\mathbf{T}_U$ and $\mathbf{T}_S$. (c) The upper sheet is under the surface tractions $\mathbf{T}_U^{Load}$ and $\mathbf{T}_U^{Self}$ and the resultant loads $\mathbf{F}$ and $\mathbf{M}$. (d) The upper nugget is under surface tractions $\mathbf{T}_C^{Load}$ and $\mathbf{T}_C^{Self}$ and the resultant loads $\mathbf{F}$ and $\mathbf{M}$.

Fig. 1(d) shows only the upper half nugget. The surface traction $\mathbf{T}_C$ along the nugget circumferential surface can be decomposed into the load-balanced part $\mathbf{T}_C^{Load}$ and the self-balanced part $\mathbf{T}_C^{Self}$ as shown in the figure. The resultant loads $\mathbf{F}$ and $\mathbf{M}$ should be statically in equilibrium with the load-balanced part $\mathbf{T}_C^{Load}$. The self-balanced part $\mathbf{T}_C^{Self}$ is statically equivalent to the self-balanced part $\mathbf{T}_U^{Self}$ on the plate lateral surface as shown in Fig. 1(c). The self-balanced surface tractions $\mathbf{T}_U^{Self}$ and $\mathbf{T}_C^{Self}$ cannot be derived in any way from the resultant loads $\mathbf{F}$ and $\mathbf{M}$. This suggests that when the resultant forces or moments from a beam or spring finite element model are used to infer the surface traction and the structural stresses on the nugget circumferential surface and the stress intensity factors along the nugget circumference, the contributions from the self-balanced surface traction on the nugget surface or the plate lateral surface cannot be accounted for.

Most researchers approximate the general loading condition of spot welds by using the resultant loads applied to the interfacial circular cross section of the weld nugget, for example, Swellam et al. (1994), Rupp et al. (1995) and Salvini et al. (2000). However, Zhang (1997, 2001), Wang et al. (2005b) and Lin et al. (2007) indicated that the closed-form stress solutions for a rigid inclusion under the self-balanced surface tractions of the plate are important to obtain the analytic solutions of the stress intensity factors for spot welds. In order to consider both the resultant loads and self-balanced surface tractions, Fig. 2 shows again the free body diagram of Fig. 1(c) for the upper sheet with the upper half nugget. The upper sheet has the thickness t and the nugget has the diameter $2a$. The Cartesian coordinate system is centered at the center of the upper half nugget located on the middle plane of the sheet. As shown in Fig. 1(c), the resultant loads on the lower surface of the upper half nugget are denoted as $\mathbf{F}$ and $\mathbf{M}$. The surface tractions in equilibrium with $\mathbf{F}$ and $\mathbf{M}$ are shown as $\mathbf{T}_U^{Load}$. As shown in Fig. 2, the resultant force $\mathbf{F}$ and the resultant moment $\mathbf{M}$ acting at the origin of the Cartesian coordinate system are now decomposed into three resultant forces F_x, F_y and F_z and three resultant moments M_x, M_y and M_z, respectively. The self-balanced resultant force $\mathbf{F}^s$ and the self-balanced resultant moment $\mathbf{M}^s$ due to the self-balance traction $\mathbf{T}_U^{Self}$ on the plate lateral surface can now be decomposed into two uniform tensile forces $\widetilde{F}_x^s$ and $\widetilde{F}_y^s$, two uniform shear forces $\widetilde{F}_{xy}^s$ and $\widetilde{F}_{yx}^s$, two uniform bending moments $\widetilde{M}_x^s$ and $\widetilde{M}_y^s$, and two uniform twisting moments $\widetilde{M}_{xy}^s$ and $\widetilde{M}_{yx}^s$.

Note that the lateral shear forces $\widetilde{F}_{xy}^s$ and $\widetilde{F}_{yx}^s$ or the lateral twisting moments $\widetilde{M}_{xy}^s$ and $\widetilde{M}_{yx}^s$ can be eliminated if the directions of the x and y axes coincide with the directions of the principal resultant forces or the principal resultant moments, respectively. However, the directions of the principal resultant forces in gen-

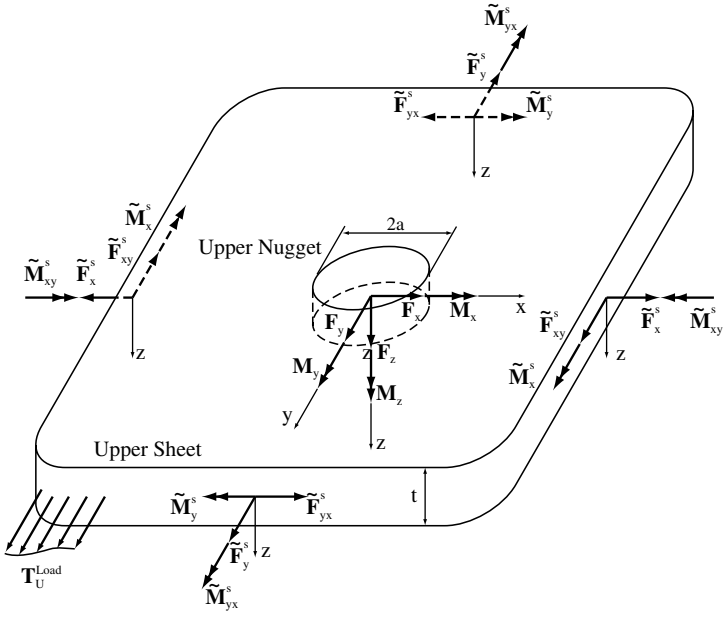

Fig. 2. The upper sheet with the upper half nugget is shown with the surface traction $\mathbf{T}_U^{Load}$, the resultant loads $\mathbf{F}$ and $\mathbf{M}$, and the self-balanced resultant loads $\mathbf{F}^s$ and $\mathbf{M}^s$. The upper sheet has the thickness t and the nugget has the diameter $2a$.

eral may not coincide with those of the principal resultant moments. Therefore, we consider both lateral shear forces and lateral twisting moments in this paper. Also note that the forces $\widetilde{F}^s_x$, $\widetilde{F}^s_y$, $\widetilde{F}^s_{xy}$, and $\widetilde{F}^s_{yx}$ and the moments $\widetilde{M}^s_x$, $\widetilde{M}^s_y$, $\widetilde{M}^s_{xy}$, and $\widetilde{M}^s_{yx}$ represent the uniformly distributed forces and moments applied to the lateral surface of the sheet. The units of the forces and moments with tilde signs are force per unit length and moment per unit length, respectively. In the following sections, we investigate the stresses, moments and transverse shear forces near a spot weld in a sheet under various types of loading conditions based on elasticity theories. Note that in the following sections, the spot weld is assumed as a rigid inclusion.

3. Elasticity theories

Within the context of elasticity theories, the stresses, moments and transverse shear forces around the circumference of a rigid inclusion in a plate can be used to derive the stress intensity factor solutions for a spot weld in a sheet under various types of loading conditions (Zhang, 1997, 2001; Lin et al., 2007). A rigid inclusion in a plate under in-plane loading conditions can be idealized as a two-dimensional plane stress problem. In this case, the Airy stress function approach can be used to derive closed-form analytical solutions. However, a rigid inclusion in a plate under bending, twisting and/or out-of-plane loading conditions is in general considered as a three-dimensional problem. Nevertheless, the classical Kirchhoff plate theory can be used to reduce the problem to be two-dimensional in the sense that the resultant forces/moments and deflections are now expressed in terms of the in-plane coordinates. It should be mentioned that for various types of specimens of interest (Lin and Pan, 2008a,b), the boundary conditions or the applied loading conditions are usually expressed in terms of the Cartesian coordinates since the shapes of the plate sections of interest in these specimens are either rectangular or square. However, the polar coordinates are adopted for the closed-formed solutions presented in the following since the rigid inclusion is circular and the closed-form solutions of interest are along the circumference of the rigid inclusion.

3.1. Airy stress function approach

First, we consider a rigid inclusion in a plate under in-plane loading conditions. The general solution is well known for this two-dimensional plane stress problem and is briefly summarized in the following. Fig. 3(a) shows the polar and Cartesian coordinate systems where the origins of both systems are located at the center of the rigid inclusion. The shaded region represents the rigid inclusion. According to the Airy stress function approach, the governing equation for the plate with a rigid inclusion can be written as a bi-harmonic equation of the Airy stress function ϕ. The governing equation in terms of the polar coordinates r and θ is

$$\nabla^4\phi \equiv \left(\frac{\partial^2}{\partial r^2}+\frac{1}{r}\frac{\partial}{\partial r}+\frac{1}{r^2}\frac{\partial^2}{\partial\theta^2}\right)\left(\frac{\partial^2\phi}{\partial r^2}+\frac{1}{r}\frac{\partial\phi}{\partial r}+\frac{1}{r^2}\frac{\partial^2\phi}{\partial\theta^2}\right)=0 \tag{1}$$

where $\nabla^4=(\nabla^2)^2$ represents the bi-harmonic operator. In the polar coordinate system, the normal and shear stresses in terms of r and θ are

$$\sigma_{rr}=\frac{1}{r}\frac{\partial\phi}{\partial r}+\frac{1}{r^2}\frac{\partial^2\phi}{\partial\theta^2} \tag{2a}$$

$$\sigma_{\theta\theta}=\frac{\partial^2\phi}{\partial r^2} \tag{2b}$$

$$\sigma_{r\theta}=-\frac{\partial}{\partial r}\left(\frac{1}{r}\frac{\partial\phi}{\partial\theta}\right) \tag{2c}$$

The general solution of Michell (1899) for Eq. (1) is

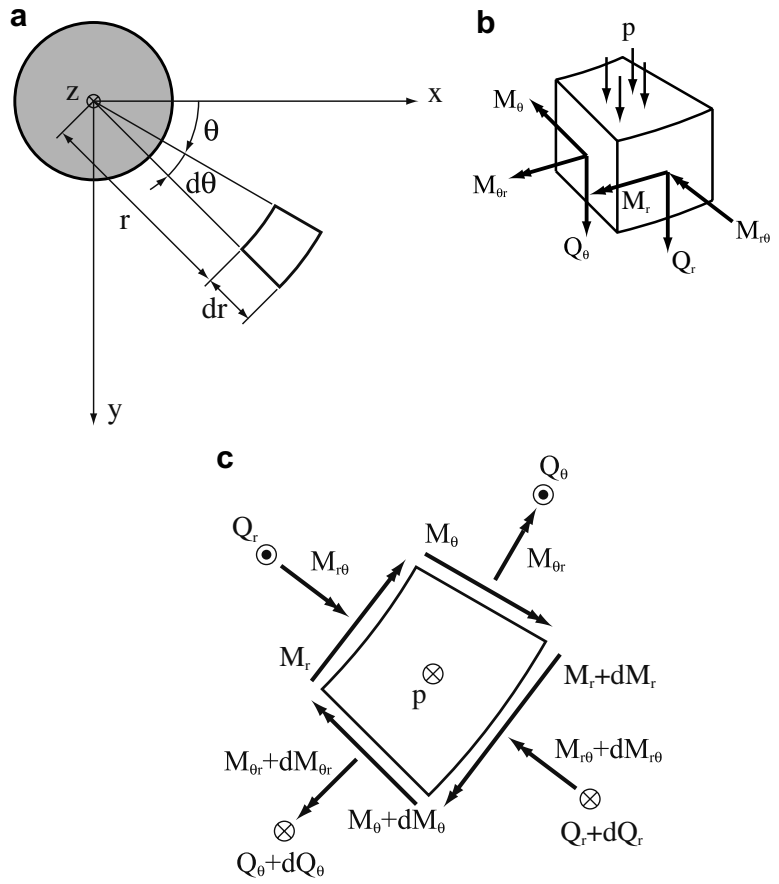

Fig. 3. (a) A top view of a differential element in a polar coordinate system, (b) a differential plate element with the radial bending moment M_r, the tangential bending moment M_θ, the twisting moments $M_{r\theta}$ and $M_{\theta r}$, the radial transverse shear force Q_r, the tangential transverse shear force Q_θ, and the distributed load p, (c) a top view of a differential plate element and the associated moments and transverse shear force.

$$\begin{aligned}\phi = {} & C_1^0 r^2 + C_2^0 r^2 \ln r + C_3^0 \ln r + C_4^0 \theta + (B_1^1 r^3 + B_1^2 r \ln r + B_1^4 r^{-1}) \cos\theta + B_1^3 r\theta \sin\theta \\ & + (C_1^1 r^3 + C_1^2 r \ln r + C_1^4 r^{-1}) \sin\theta + C_1^3 r\theta \cos\theta + \sum_{n=2}^{\infty} (B_n^1 r^{n+2} + B_n^2 r^{-n+2} + B_n^3 r^n + B_n^4 r^{-n}) \cos n\theta \\ & + \sum_{n=2}^{\infty} \left(C_n^1 r^{n+2} + C_n^2 r^{-n+2} + C_n^3 r^n + C_n^4 r^{-n}\right) \sin n\theta \end{aligned} \tag{3}$$

where B_n^i and C_n^i are the unknown coefficients which can be determined to satisfy the boundary conditions for each particular case.

3.2. Kirchhoff plate theory

Now we consider a rigid inclusion in a plate under bending, twisting and/or out-of-plane loading conditions. Fig. 3(a) can be used to represent a top view of a rigid inclusion in a plate with both polar and Cartesian coordinate systems centered at the center of the inclusion on the mid-plane of the plate. Fig. 3(b) shows a differential plate element with the radial bending moment M_r, the tangential bending moment M_θ, the twisting moments $M_{r\theta}$ and $M_{\theta r}$, the radial transverse shear force Q_r, the tangential transverse shear force Q_θ, and the distributed load p. Fig. 3(c) shows a top view of a differential plate element and the moments and transverse

shear forces. The symbols "cross" and "dot" indicate the direction in the positive z and negative z directions, respectively.

According to the Kirchhoff plate theory (Timoshenko and Woinowsky-Krieger, 1959), the governing equation for a plate without a distributed load p on the plate surface can be written as a bi-harmonic equation of the plate transverse deflection ω. The governing equation in terms of the polar coordinates r and θ is

$$\nabla^4\omega \equiv \left(\frac{\partial^2}{\partial r^2}+\frac{1}{r}\frac{\partial}{\partial r}+\frac{1}{r^2}\frac{\partial^2}{\partial\theta^2}\right)\left(\frac{\partial^2\omega}{\partial r^2}+\frac{1}{r}\frac{\partial\omega}{\partial r}+\frac{1}{r^2}\frac{\partial^2\omega}{\partial\theta^2}\right)=0 \tag{4}$$

In the polar coordinate system, the moments and transverse shear forces in terms of r and θ are

$$M_r=-D\left[\frac{\partial^2\omega}{\partial r^2}+v\left(\frac{1}{r}\frac{\partial\omega}{\partial r}+\frac{1}{r^2}\frac{\partial^2\omega}{\partial\theta^2}\right)\right] \tag{5a}$$

$$M_\theta=-D\left(\frac{1}{r}\frac{\partial\omega}{\partial r}+\frac{1}{r^2}\frac{\partial^2\omega}{\partial\theta^2}+v\frac{\partial^2\omega}{\partial r^2}\right) \tag{5b}$$

$$M_{r\theta}=M_{\theta_r}=-(1-v)D\left(\frac{1}{r}\frac{\partial^2\omega}{\partial r\partial\theta}-\frac{1}{r^2}\frac{\partial\omega}{\partial\theta}\right) \tag{5c}$$

$$Q_r=-D\frac{\partial}{\partial r}(\nabla\omega) \tag{5d}$$

$$Q_\theta=-D\frac{\partial(\nabla\omega)}{r\partial\theta} \tag{5e}$$

where D is the flexural rigidity of the plate and v is the Poisson's ratio. The flexural rigidity of the plate D is defined as

$$D=\frac{Et^3}{12(1-v^2)} \tag{6}$$

where E is the Young's modulus and t is the thickness of the plate. The corresponding normal and shear stresses as functions of the out-of-plane coordinate z are

$$\sigma_{rr}=\frac{M_r z}{I} \tag{7a}$$

$$\sigma_{\theta\theta}=\frac{M_\theta z}{I} \tag{7b}$$

$$\tau_{r\theta}=\frac{M_{r\theta} z}{I} \tag{7c}$$

$$\tau_{zr}=\frac{Q_r}{2I}\left(\frac{t^2}{4}-z^2\right) \tag{7d}$$

$$\tau_{z\theta}=\frac{Q_\theta}{2I}\left(\frac{t^2}{4}-z^2\right) \tag{7e}$$

where I ($=t^3/12$) is the moment of inertia per unit length. The general solution of ω in Eq. (4) is

$$\omega=R_0+\sum_{m=1}^{\infty}R_m\cos m\theta+\sum_{m=1}^{\infty}R'_m\sin m\theta \tag{8}$$

where R_0, R_m and R'_m are functions of the radial distance r. Here, R_0 and R_1 are

$$R_0=A_0+B_0r^2+C_0\ln r+D_0r^2\ln r \tag{9}$$

$$R_1=A_1r+B_1r^3+C_1r^{-1}+D_1r\ln r \tag{10}$$

where A_0, B_0, C_0, D_0, A_1, B_1, C_1, and D_1 are unknown coefficients. The general form of the function R_m for $m>1$ is

$$R_m = A_m r^m + B_m r^{-m} + C_m r^{m+2} + D_m r^{-m+2} \tag{11}$$

where A_m, B_m, C_m and D_m are unknown coefficients. Similar expressions can be written for the function R'_m. Substituting Eqs. (9)–(11) for the functions R_m and the corresponding equations for the functions R'_m into Eq. (8), we can obtain the general solution of ω. The unknown coefficients A_m, B_m, C_m, D_m, A'_m, B'_m, C'_m, and D'_m can be determined to satisfy the boundary conditions for each particular case.

4. Closed-form solutions for resultant forces and moments on inclusions

Closed-form solutions for plates with inclusions under different resultant forces and moments are summarized in this section. The solutions are needed to derive the new closed-form stress intensity factor solutions for spot welds in five commonly used specimens as detailed in a subsequent paper (Lin and Pan, 2008a).

4.1. Shear forces F_x and F_y

Fig. 4(a) shows a two-dimensional model of an infinite plate with a rigid inclusion subjected to a resultant shear force F_x to the rigid inclusion. This model represents a spot weld under shear loading conditions. In this figure, the shaded circle represents a rigid inclusion of the radius a. As shown in the figure, a Cartesian coordinate system is centered at the center of the inclusion. The shear force F_x, marked as an arrow in the positive x direction, represents the resultant force acting to the inclusion. The shear force F_x moves the rigid inclusion

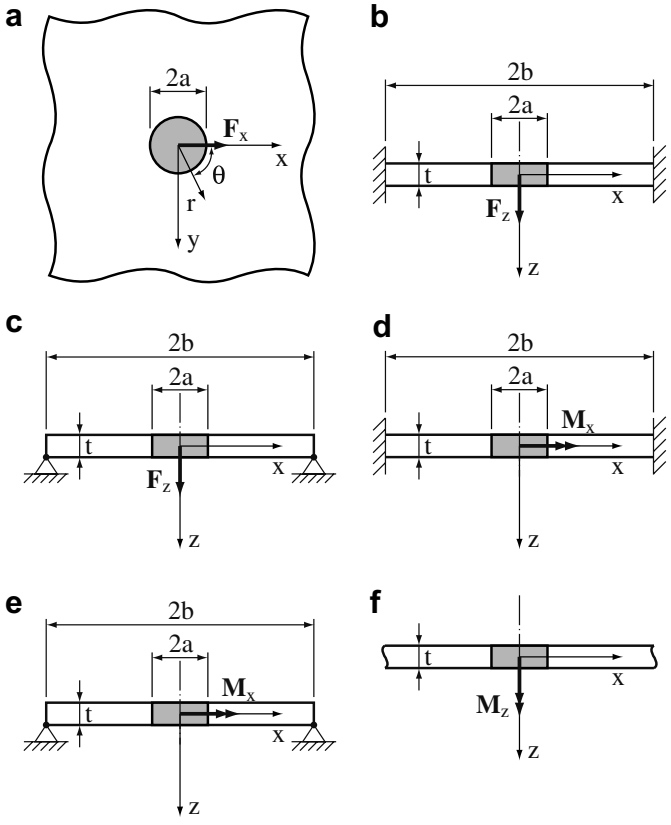

Fig. 4. A plate with a rigid inclusion subjected to various types of resultant loads to the inclusion and subjected to different types of boundary conditions. (a) A shear force F_x, (b) an opening force F_z and a clamped edge, (c) an opening force F_z and a simply supported edge, (d) a central bending moment M_x and a clamped edge, (e) a central bending moment M_x and a simply supported edge, and (f) a twisting moment M_z.

by a displacement δ in the positive x direction. The rigid inclusion represents the spot weld nugget and the infinite plate represents the sheet surrounding the spot weld nugget. Here, the inclusion is assumed to be perfectly bonded to the plate at $r = a$ and the stresses and strains are assumed to be zero at infinity. For all models considered in this paper, the inclusion is assumed to be perfectly bonded to the neighboring plate.

A polar coordinate system centered at the center of the rigid inclusion is also considered here for convenience. The displacement boundary conditions along the inclusion circumference give the displacements at $r = a$ as

$$u_r = \delta \cos\theta \tag{12}$$

$$u_\theta = -\delta \sin\theta \tag{13}$$

where u_r and u_θ represent the displacements in the radial and tangential directions, respectively, and δ is the rigid-body displacement in the positive x direction. The weak boundary condition along the circumference of the rigid inclusion at $r = a$ gives the equilibrium equation as

$$\int_0^{2\pi} (\sigma_{rr}\cos\theta - \sigma_{r\theta}\sin\theta) rt \mathrm{d}\theta = -F_x \tag{14}$$

It is straightforward to solve the two-dimensional elastic boundary valued problem by the Airy stress function approach using the general solution of Michell (1899). The stresses in the infinite plate are given as

$$\sigma_{rr} = F_x \left[-\frac{(3+\nu)}{4\pi rt} + \frac{(1+\nu)a^2}{4\pi r^3 t} \right] \cos\theta \tag{15a}$$

$$\sigma_{r\theta} = F_x \left[\frac{(1-\nu)}{4\pi rt} + \frac{(1+\nu)a^2}{4\pi r^3 t} \right] \sin\theta \tag{15b}$$

$$\sigma_{\theta\theta} = F_x \left[\frac{(1-\nu)}{4\pi rt} - \frac{(1+\nu)a^2}{4\pi r^3 t} \right] \cos\theta \tag{15c}$$

The closed-form solutions of this model were also presented in Muskhelishvili (1953) based on the complex variable approach and Lin et al. (2006) based on the Airy stress function approach. Zhang (1997) used this solution to obtain the mode II and III stress intensity factors for spot welds in lap-shear specimens. As shown in Wang et al. (2005b) and Lin et al. (2006), this solution is applicable for a lap-shear specimen with the ratio of the specimen width to the nugget diameter as small as 5. An approximate closed-form solution for a finite circular plate containing a rigid inclusion with a clamped edge was presented by Salvini et al. (2000). Note that the stresses for the spot weld under the resultant shear force F_y can be obtained by substituting $\theta + \pi/2$ for θ in Eq. (15).

4.2. Opening force F_z

Fig. 4(b) shows an axisymmetric model of a finite circular plate with a clamped edge. The plate contains a rigid inclusion subjected to a resultant opening force F_z. This model represents a spot weld under opening loading conditions. The opening force F_z, marked as an arrow in the positive z direction, represents the resultant force acting on the inclusion. Note that the specimen width is important to the structural stresses for spot welds under opening loading conditions (Wang et al., 2005a). Therefore, we take a finite circular plate here instead of an infinite plate. In this figure, the circular plate with a diameter $2b$ represents the bottom sheet of the upper cup or the top sheet of the lower cup of a circular-cup specimen (Wang et al., 2005a). The edge of the circular plate is considered to be clamped due to the sharp flange along the edge of the circular bottom and top sheets of the upper and lower cups, respectively.

The displacement boundary condition along the inclusion circumference at $r = a$ is given as

$$\left(\frac{\partial\omega}{\partial r}\right)_{r=a} = 0 \tag{16}$$

The displacement boundary conditions along the plate circumference at $r = b$ are given as

$$(\omega)_{r=b} = 0 \tag{17}$$

$$\left(\frac{\partial \omega}{\partial r}\right)_{r=b} = 0 \tag{18}$$

The boundary condition gives the equilibrium equation for any given r as

$$\widetilde{Q}_r = \frac{-F_z}{2\pi r} \tag{19}$$

It is straightforward to derive the closed-form solutions for this model based on the classical Kirchhoff plate theory. The moments and shear forces in the plate are given as

$$\widetilde{M}_r = \frac{-F_z}{4\pi r^2(a^2-b^2)}\{b^2[-a^2(-1+\nu)+r^2(1+\nu)]\ln(b/a) + (a^2-b^2)r^2[1+(1+\nu)\ln(r/a)]\} \tag{20a}$$

$$\widetilde{M}_{r\theta} = 0 \tag{20b}$$

$$\widetilde{M}_\theta = \frac{-F_z}{4\pi r^2(a^2-b^2)}\{b^2[a^2(-1+\nu)+r^2(1+\nu)]\ln(b/a) + (a^2-b^2)r^2[\nu+(1+\nu)\ln(r/a)]\} \tag{20c}$$

$$\widetilde{Q}_r = \frac{-F_z}{2\pi r} \tag{20d}$$

$$\widetilde{Q}_\theta = 0 \tag{20e}$$

The corresponding stresses can be derived by substituting Eq. (20) into Eq. (7). This solution was listed in Young and Budynas (2002). Pook (1979) and Wang et al. (2005a) used this solution to derive the mode I stress intensity factor solution for circular plates with connection and circular-cup specimens.

Fig. 4(c) shows an axisymmetric model of a circular plate with a simply supported edge. The plate contains a rigid inclusion subjected to a resultant opening force F_z. The displacement boundary condition along the inclusion circumference at $r = a$ and the weak boundary condition for equilibrium are identical to those in Eqs. (16) and (19). With consideration of the simply supported edge, the boundary conditions along the circumference of the plate at $r = b$ are given as

$$(\omega)_{r=b} = 0 \tag{21}$$

$$(M_r)_{r=b} = 0 \tag{22}$$

Based on the classical Kirchhoff plate theory, the moments and shear forces of this model are given as

$$\widetilde{M}_r = \frac{F_z}{4\pi r^2[a^2(-1+\nu)-b^2(1+\nu)]}\{a^2(b^2-r^2)(-1+\nu) + b^2(1+\nu)[a^2(-1+\nu)-r^2(1+\nu)]\ln(b/a) + r^2[b^2(1+\nu)^2-a^2(-1+\nu^2)]\ln(r/a)\} \tag{23a}$$

$$\widetilde{M}_{r\theta} = 0 \tag{23b}$$

$$\widetilde{M}_\theta = \frac{-F_z}{4\pi r^2[a^2(-1+\nu)-b^2(1+\nu)]}\{(-1+\nu)[-b^2r^2(1+\nu)+a^2(b^2+r^2\nu)] + b^2(1+\nu)[a^2(-1+\nu)+r^2(1+\nu)]\ln(b/a) + r^2(1+\nu)[a^2(-1+\nu)-b^2(1+\nu)]\ln(r/a)\} \tag{23c}$$

$$\widetilde{Q}_r = \frac{-F_z}{2\pi r} \tag{23d}$$

$$\widetilde{Q}_\theta = 0 \tag{23e}$$

The corresponding stresses can be derived by substituting Eq. (23) into Eq. (7). This solution was listed in Young and Budynas (2002). Pook (1979) used this solution to derive the mode I stress intensity factor solution for circular plates with connection. Lin and Pan (2008a) used this solution to derive the stress intensity factor solutions for various types of specimens.

4.3. Central bending moments M_x and M_y

Fig. 4(d) shows a model of a finite circular plate with a clamped edge. The plate contains a rigid inclusion subjected to a central bending moment M_x. This model represents a spot weld under central bending conditions. The central bending moment M_x, marked as an arrow in the positive x direction, represents the resultant bending moment acting on the inclusion. The displacement boundary condition along the inclusion circumference at $r = a$ due to the rotation of the rigid inclusion based on the geometry is given as

$$\left(\frac{\partial\omega}{\partial r}\right)_{r=a} = \left(\frac{\omega}{r}\right)_{r=a} \tag{24}$$

The displacement boundary conditions along the circumference of the plate at $r = b$ are given as

$$(\omega)_{r=b} = 0 \tag{25}$$

$$\left(\frac{\partial\omega}{\partial r}\right)_{r=b} = 0 \tag{26}$$

The weak boundary condition gives the equilibrium equation for any given r as

$$\int_0^{2\pi} (M_r r\sin\theta - Q_r r^2\sin\theta + M_{r\theta} r\cos\theta)\mathrm{d}\theta = -M_x \tag{27}$$

It is straightforward to derive the closed-form solutions of this model based on the classical Kirchhoff plate theory. The detailed derivations for this problem were presented in Reißner (1929). The moments and shear forces of this model are given as

$$\widetilde{M}_r = \frac{M_x\{a^2[b^2(-1+\nu) - r^2(1+\nu)] + r^2[-b^2(1+\nu) + r^2(3+\nu)]\}\sin\theta}{4\pi r^3(a^2+b^2)} \tag{28a}$$

$$\widetilde{M}_{r\theta} = \frac{M_x(a^2-r^2)(b^2-r^2)(1-\nu)\cos\theta}{4\pi r^3(a^2+b^2)} \tag{28b}$$

$$\widetilde{M}_\theta = \frac{M_x\{a^2[b^2(1-\nu) - r^2(1+\nu)] + r^2[-b^2(1+\nu) + r^2(1+3\nu)]\}\sin\theta}{4\pi r^3(a^2+b^2)} \tag{28c}$$

$$\widetilde{Q}_r = \frac{M_x(a^2+b^2+2r^2)\sin\theta}{2\pi r^2(a^2+b^2)} \tag{28d}$$

$$\widetilde{Q}_\theta = \frac{-M_x(a^2+b^2-2r^2)\cos\theta}{2\pi r^2(a^2+b^2)} \tag{28e}$$

Note that when $b \gg a$, the closed-form solutions of the finite plate model in Eq. (28) can be used to approximate those for an infinite plate with a rigid inclusion. The limits of the moments and shear forces of the finite plate model in Eq. (28) for $b \gg a$ are given as

$$\widetilde{M}_r = \frac{M_x[a^2(-1+v) - r^2(1+v)]\sin\theta}{4\pi r^3} \tag{29a}$$

$$\widetilde{M}_{r\theta} = \frac{M_x(a^2 - r^2)(1-v)\cos\theta}{4\pi r^3} \tag{29b}$$

$$\widetilde{M}_\theta = \frac{M_x[a^2(1-v) - r^2(1+v)]\sin\theta}{4\pi r^3} \tag{29c}$$

$$\widetilde{Q}_r = \frac{M_x\sin\theta}{2\pi r^2} \tag{29d}$$

$$\widetilde{Q}_\theta = \frac{-M_x\cos\theta}{2\pi r^2} \tag{29e}$$

Zhang (1997) used this solution to derive the mode II stress intensity factor solution for lap-shear specimens. Zhang (1997) also used this solution to approximate the solution under counter bending conditions to derive the mode I stress intensity factor solutions for lap-shear and cross-tension specimens.

Fig. 4(e) shows a model of a finite circular plate with a simply supported edge. The plate contains a rigid inclusion subjected to a central bending moment M_x. This model represents a spot weld under central bending conditions. The boundary condition along the inclusion circumference at $r = a$ and the weak boundary condition for equilibrium equation are identical to those in Eqs. (24) and (27), respectively. The boundary conditions along the circumference of the plate at $r = b$ are given as

$$(\omega)_{r=b} = 0 \tag{30}$$

$$(\widetilde{M}_r)_{r=b} = 0 \tag{31}$$

It is straightforward to derive the closed-form solutions of this model based on the classical Kirchhoff plate theory. The detailed derivations of the solutions were presented in Timoshenko and Woinowsky-Krieger (1959). The moments and shear forces of this model are given as

$$\begin{aligned}\widetilde{M}_r = {} & \frac{M_x(b^2 - r^2)}{4\pi r^3[a^4(-1+v) - b^4(3+v)]}[a^4(-1+v^2) \\ & - a^2(b^2+r^2)(-3+2v+v^2) + b^2r^2(3+4v+v^2)]\sin\theta\end{aligned} \tag{32a}$$

$$\begin{aligned}\widetilde{M}_{r\theta} = {} & \frac{M_x(a^2 - r^2)(1-v)}{4\pi r^3[a^4(-1+v) - b^4(3+v)]}\{a^2[r^2(1-v) + b^2(1+v)] \\ & + b^2[r^2(1+v) - b^2(3+v)]\}\cos\theta\end{aligned} \tag{32b}$$

$$\begin{aligned}\widetilde{M}_\theta = {} & \frac{M_x}{4\pi r^3[a^4(-1+v) - b^4(3+v)]}\{a^4(b^2+r^2)(1-v^2) \\ & + b^2r^2(1+v)[b^2(3+v) - r^2(1+3v)] \\ & + a^2[b^4(-3+2v+v^2) + r^4(-1-2v+3v^2)]\}\sin\theta\end{aligned} \tag{32c}$$

$$\begin{aligned}\widetilde{Q}_r = {} & \frac{M_x}{2\pi r^2[a^4(-1+v) - b^4(3+v)]}\{a^4(-1+v) + 2a^2r^2(-1+v) \\ & - b^2[2r^2(1+v) + b^2(3+v)]\}\sin\theta\end{aligned} \tag{32d}$$

$$\begin{aligned}\widetilde{Q}_\theta = {} & \frac{M_x}{2\pi r^2[a^4(-1+v) - b^4(3+v)]}\{-a^4(-1+v) + 2a^2r^2(-1+v) \\ & + b^2[-2r^2(1+v) + b^2(3+v)]\}\cos\theta\end{aligned} \tag{32e}$$

Note that the moments and shear forces for the resultant moment M_y can be obtained by substituting $\theta + \pi/2$ for θ in Eqs. (28), (29), or (32). The corresponding stresses can be derived by substituting Eqs. (28), (29), or (32) into Eq. (7). Lin and Pan (2008a) used this solution to derive a new mode I stress intensity factor solution for coach-peel specimens.

4.4. Twisting moment M_z

Fig. 4(f) shows an axisymmetric model of an infinite plate with a rigid inclusion subjected to a twisting moment M_z. This model represents a spot weld under twisting loading conditions. The twisting moment M_z, marked as an arrow in the positive z direction, represents the resultant twisting moment acting on the inclusion. Based on the elementary solid mechanics, the closed-form solution of this model is given as

$$\tau_{r\theta} = \frac{-M_z}{2\pi r^2 t} \tag{33}$$

Zhang (1999, 2001) used this solution to derive the mode III stress intensity factor solution.

5. Closed-form solutions for self-balanced resultant forces and moments on plate lateral surface

Closed-form solutions for plates with inclusions under different self-balanced resultant forces and moments are summarized in the following. Note that the solutions are needed to derive the new closed-form stress inten-

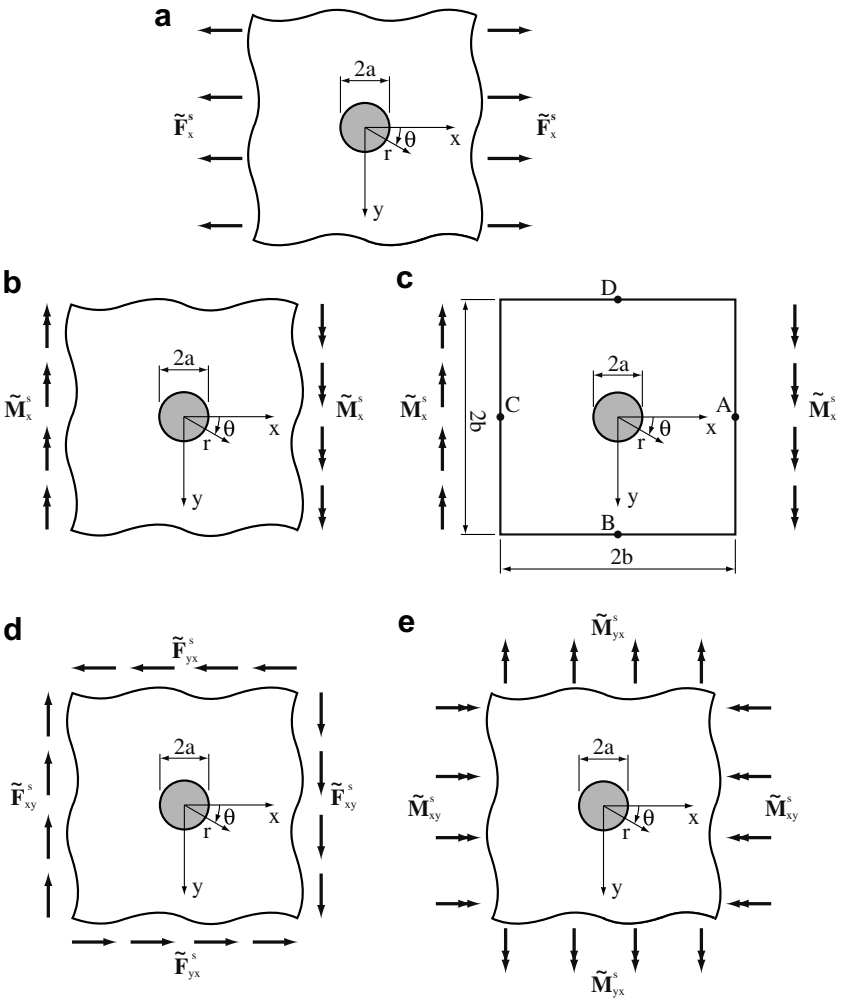

Fig. 5. A plate with a rigid inclusion subjected to various types of self-balanced resultant loads on the plate lateral surface. (a) A remote uniform tensile force $\tilde{F}^s_x$, (b) a remote uniform counter bending moment $\tilde{M}^s_x$, (c) a uniform counter bending moment $\tilde{M}^s_x$ along two edges of a square plate, (d) a remote uniform shear force $\tilde{F}^s_{xy}$, and (e) a remote uniform twisting moment $\tilde{M}^s_{xy}$.

sity factor solutions for five commonly used spot weld specimens as detailed in a subsequent paper (Lin and Pan, 2008a).

5.1. Self-balanced tensile/compressive force $\widetilde{F}_x^s$ and $\widetilde{F}_y^s$

Fig. 5(a) shows a model of an infinite plate with a rigid inclusion subjected to a remote uniformly distributed tensile force $\widetilde{F}_x^s$. This model represents a spot weld under tensile/compressive loading conditions. This rigid inclusion problem can be considered as a two-dimensional plane stress problem. The displacement boundary conditions at $r = a$ along the circumference of the inclusion are expressed as

$$u_r = 0 \tag{34}$$

$$u_\theta = 0 \tag{35}$$

where u_r and u_θ represent the displacements in the radial and tangential directions, respectively. It is straightforward to solve the two-dimensional elastic boundary valued problem by the Airy stress function approach using the general solution of Michell (1899). The stresses in the infinite plate are given as

$$\sigma_{rr} = \frac{\widetilde{F}_x^s}{t}\left\{\left[\frac{1}{2}+\frac{a^2(1-\nu)}{2r^2(1+\nu)}\right]+\left[\frac{1}{2}-\frac{2a^2(1+\nu)}{r^2(-3+\nu)}+\frac{3a^4(1+\nu)}{2r^4(-3+\nu)}\right]\cos(2\theta)\right\} \tag{36a}$$

$$\sigma_{r\theta} = \frac{\widetilde{F}_x^s}{t}\left[\frac{-1}{2}-\frac{a^2(1+\nu)}{r^2(-3+\nu)}+\frac{3a^4(1+\nu)}{2r^4(-3+\nu)}\right]\sin(2\theta) \tag{36b}$$

$$\sigma_{\theta\theta} = \frac{\widetilde{F}_x^s}{t}\left\{\left[\frac{1}{2}+\frac{a^2(-1+\nu)}{2r^2(1+\nu)}\right]-\left[\frac{1}{2}+\frac{3a^4(1+\nu)}{2r^4(-3+\nu)}\right]\cos(2\theta)\right\} \tag{36c}$$

Note that the stresses for $\widetilde{F}_y^s$ can be obtained by substituting $\theta + \pi/2$ for θ in Eq. (36). Note that the r-dependent terms on the right-hand sides of Eqs. (36a), (36b) and (36c) are expressed in terms of $(a/r)^2$ and $(a/r)^4$. The constant terms on the right-hand sides of Eqs. (36a), (36b) and (36c) are in general related to the constant remote uniform tensile force in the x direction. When a/r is less than 0.1, the contributions of these terms are a few percents of the constant terms in the order of unity, and the stress state at this radial distance r can be used to approximate the self-balanced tensile/compressive loading for a finite square plate with a rigid inclusion. Therefore, the solutions in Eq. (36) can be approximately applicable to a rigid inclusion in a square plate of the width $2b$ where b/a is larger than 10.

5.2. Self-balanced counter bending moment $\widetilde{M}_x^s$ and $\widetilde{M}_y^s$

Fig. 5(b) shows a model of an infinite plate with a rigid inclusion subjected to a remote uniform counter bending moment $\widetilde{M}_x^s$. This model represents a spot weld under counter bending loading conditions. Based on the assumptions of the rigid inclusion and the perfect bonding between the inclusion and the neighboring plate, the displacement boundary conditions along the circumference of the inclusion at $r = a$ are given as

$$(\omega)_{r=a} = 0 \tag{37}$$

$$\left(\frac{\partial\omega}{\partial r}\right)_{r=a} = 0 \tag{38}$$

The boundary conditions along the remote edges of the plate for this model are

$$(M_x)_{x\to\pm\infty} = \widetilde{M}_x^s \tag{39}$$

$$(M_y)_{y\to\pm\infty} = 0 \tag{40}$$

It is straightforward to derive the closed-form solutions of this model based on the classical Kirchhoff plate theory. The detailed derivations of the solutions were presented in Goland (1943) and Lin et al. (2007). The moments and shear forces of this model are given as

$$\widetilde{M}_r = \frac{\widetilde{M}_x^s}{2r^4(-1+v^2)}\{r^2(-1+v)[-a^2(-1+v)+r^2(1+v)] + (1+v)[3a^4(-1+v)+r^4(-1+v)-4a^2r^2v]\cos 2\theta\} \tag{41a}$$

$$\widetilde{M}_{r\theta} = \frac{-\widetilde{M}_x^s}{2r^4}(-3a^4+2a^2r^2+r^4)\sin 2\theta \tag{41b}$$

$$\widetilde{M}_\theta = \frac{\widetilde{M}_x^s}{2r^4(-1+v^2)}\{r^2(-1+v)[a^2(-1+v)+r^2(1+v)] - (1+v)[4a^2r^2+3a^4(-1+v)+r^4(-1+v)]\cos 2\theta\} \tag{41c}$$

$$\widetilde{Q}_r = \frac{4\widetilde{M}_x^s a^2\cos 2\theta}{r^3(-1+v)} \tag{41d}$$

$$\widetilde{Q}_\theta = \frac{4\widetilde{M}_x^s a^2\sin 2\theta}{r^3(-1+v)} \tag{41e}$$

By the similar argument for the case of a plate with a rigid inclusion under self-balanced tensile/compressive forces, the moment solutions in Eq. (41) should be approximately valid for a rigid inclusion in a square plate of the width $2b$ where b/a is larger than 10.

Fig. 5(c) shows a model of a finite square plate with a rigid inclusion subjected to a uniform counter bending moment $\widetilde{M}_x^s$ along the two edges as shown. In this figure, the square plate has the size of $2b$ as shown. The size $2b$ can be correlated to the widths of various types of specimens as shown in Lin and Pan (2008a). The displacement boundary conditions along the inclusion circumference at $r = a$ are identical to Eqs. (37) and (38). The boundary conditions along the edges of the plate are

$$(M_x)_{x=\pm b} = \widetilde{M}_x^s, \quad (M_{xy})_{x=\pm b} = 0, \quad (Q_x)_{x=\pm b} = 0 \tag{42}$$

$$(M_y)_{y=\pm b} = 0, \quad (M_{yx})_{y=\pm b} = 0, \quad (Q_y)_{y=\pm b} = 0 \tag{43}$$

However, it is very difficult to apply the boundary conditions in Eqs. (42) and (43) to determine the coefficients of the solution of ω with respect to the polar coordinate system. Therefore, Lin et al. (2007) selected a set of approximate boundary conditions at points A, B, C, and D on the edges of the plate as shown in Fig. 5(c). Based on the boundary conditions in Eqs. (42) and (43), the approximate boundary conditions at point A ($r = b$, $\theta = 0°$) are selected to be

$$(M_r)_{r=b,\theta=0°} = \widetilde{M}_x^s \tag{44}$$

$$(Q_r)_{r=b,\theta=0°} = 0 \tag{45}$$

The approximate boundary conditions at point B ($r = b$, $\theta = 90°$) are selected to be

$$(M_r)_{r=b,\theta=90°} = 0 \tag{46}$$

$$(Q_r)_{r=b,\theta=90°} = 0 \tag{47}$$

Due to the symmetry, the approximate boundary conditions at points C and D are not shown here. Note that $M_{r\theta}$ in the rightward and downward directions of the inclusion ($\theta = 0°$ and 90°) is identically zero due to symmetry. Therefore, $M_{r\theta}$ is not considered in the approximate boundary conditions.

With consideration of the approximate boundary conditions, it is straightforward to derive the approximate closed-form solutions of this model based on the classical Kirchhoff plate theory. The detailed derivation for the solutions was presented in Lin et al. (2007). The moments and shear forces of this model are listed here as

$$\widetilde{M}_r = \frac{\widetilde{M}^s_x}{2r^4XY}\{r^2X[r^2Y + a^2(b^2 - r^2)(-1+\nu)] + Y[r^4X + a^8(b^4 - r^4)(-1+\nu) + 3a^4b^4(b^4 - r^4)(-1+\nu) - 4a^2b^4r^2(b^2 - r^2)(-r^2 + b^2\nu)]\cos 2\theta\} \tag{48a}$$

$$\widetilde{M}_{r\theta} = \frac{\widetilde{M}^s_x b^4(a^2 - r^2)[a^6 + r^2(a^4 + b^4) + a^2(3b^4 + 2r^4)](-1+\nu)\sin 2\theta}{2r^4X} \tag{48b}$$

$$\widetilde{M}_\theta = \frac{-\widetilde{M}^s_x}{2r^4XY}\{r^2X[-r^2Y + a^2(b^2 + r^2)(-1+\nu)] + Y[r^4X + a^8(b^4 - r^4)(-1+\nu) + 3a^4b^4(b^4 - r^4)(-1+\nu) + 4a^2b^4r^2(b^2 + r^2)(b^2 + r^2\nu)]\cos 2\theta\} \tag{48c}$$

$$\widetilde{Q}_r = \frac{4\widetilde{M}^s_x a^2b^4(b^4 - r^4)\cos 2\theta}{r^3X} \tag{48d}$$

$$\widetilde{Q}_\theta = \frac{4\widetilde{M}^s_x a^2b^4(b^4 + r^4)\sin 2\theta}{r^3X} \tag{48e}$$

where X and Y are defined as

$$X = (-1+\nu)(a^4 + b^4)^2 - 4a^2b^6(1+\nu) \tag{49a}$$

$$Y = a^2(-1+\nu) - b^2(1+\nu) \tag{49b}$$

Note that the moments and shear forces for the counter bending moment $\widetilde{M}^s_y$ can be derived by substituting $\theta + \pi/2$ for θ in Eqs. (41) and (48). The corresponding stresses can be derived by substituting Eqs. (41) and (48) into Eq. (7). This solution appears to be approximately valid for b/a as small as 5 (Lin et al., 2007) by comparing the moments and shear forces based on the closed-form solution and those of the applied counter bending conditions along the four edges of a square plate with various ratios of b/a. Additionally, we performed a three-dimensional finite element analysis of a finite square plate with a rigid inclusion under counter bending conditions. Counter bending moments were applied to the two opposite edges of the square plate as shown in Fig. 5(c). The computational results were obtained for a large ratio of $b/a = 25$ and a small ratio $b/a = 6$ with $t/a = 0.2$ and $\nu = 0.3$. The difference of the computational result and the closed-form solution for the maximum $\widetilde{M}_r$ at the critical locations ($\theta = 0$ or π as shown Fig. 5(c)) along the inclusion circumference for the large ratio of $b/a = 25$ is less than 1%. For the small ratio of $b/a = 6$, the difference of the computational result and the closed-form solution for the maximum $\widetilde{M}_r$ at the critical locations along the inclusion circumference is less than 5%. The computational results suggest that the closed-form solution is approximately valid for b/a as small as 6. Note that this solution is the key to derive the closed-form stress intensity factor solutions for various types of specimens in the subsequent paper (Lin and Pan, 2008a) since the sizes of these specimens are critical for the solutions.

5.3. Self-balanced shear forces $\widetilde{F}^s_{xy}$ and $\widetilde{F}^s_{yx}$

Fig. 5(d) shows a model of an infinite plate with a rigid inclusion subjected to remote uniform shear forces $\widetilde{F}^s_{xy}$ and $\widetilde{F}^s_{yx}$. Note that $\widetilde{F}^s_{xy}$ and $\widetilde{F}^s_{yx}$ should be the identical due to equilibrium. Based on the Mohr's circle transformation, the lateral shear loading condition is equivalent to a combined tensile and compressive loading condition in a new x' and y' coordinate system where $\widetilde{F}^s_{x'} = \widetilde{F}^s_{xy}$ and $\widetilde{F}^s_{y'} = -\widetilde{F}^s_{xy}$. The x' and y' axes are rotated 45° counterclockwise from the original x and y axes, respectively. Substituting $\widetilde{F}^s_{xy}$ for $\widetilde{F}^s_x$ and $\theta + \pi/4$ for θ in Eq. (36) gives the stresses under tensile loading conditions and substituting $-\widetilde{F}^s_{xy}$ for $\widetilde{F}^s_x$ and $\theta + 3\pi/4$ for θ in Eq. (36) gives the stresses under compressive loading conditions. Then combining the stresses under tensile and compressive loading conditions gives the stresses of this model as

$$\sigma_{rr} = \frac{-\widetilde{F}^s_{xy}}{r^4 t(-3+\nu)}[r^4(-3+\nu) + (3a^4 - 4a^2r^2)(1+\nu)]\sin 2\theta \tag{50a}$$

$$\sigma_{r\theta} = \frac{\widetilde{F}^s_{xy}}{r^4 t(-3+\nu)}[-r^4(-3+\nu) + (3a^4 - 2a^2r^2)(1+\nu)]\cos 2\theta \tag{50b}$$

$$\sigma_{\theta\theta} = \frac{\widetilde{F}^s_{xy}}{r^4 t(-3+\nu)}[r^4(-3+\nu) + 3a^4(1+\nu)]\sin 2\theta \tag{50c}$$

By the similar argument for the case of a plate with a rigid inclusion under self-balanced tensile/compressive forces, the solutions in Eq. (50) should be approximately valid for a rigid inclusion in a square plate of the width $2b$ where b/a is larger than 10.

5.4. Self-balanced twisting moments $\widetilde{M}^s_{xy}$ and $\widetilde{M}^s_{yx}$

Fig. 5(e) shows a model of an infinite plate with a rigid inclusion subjected to remote uniform twisting moments $\widetilde{M}^s_{xy}$ and $\widetilde{M}^s_{yx}$. Note that $\widetilde{M}^s_{xy}$ and $\widetilde{M}^s_{yx}$ should be identical due to equilibrium. Based on the Mohr's circle transformation, the twisting loading condition is equivalent to a combined counter bending loading condition in a new x' and y' coordinate system where $\widetilde{M}^s_{x'} = \widetilde{M}^s_{xy}$ and $\widetilde{M}^s_{y'} = -\widetilde{M}^s_{xy}$. The x' and y' axes are rotated 45° counterclockwise from the original x and y axes, respectively. Substituting $\widetilde{M}^s_{xy}$ for $\widetilde{M}^s_x$ and $\theta + \pi/4$ for θ in Eq. (41) or (48) gives one set of the moments and forces under counter bending loading conditions and substituting $-\widetilde{M}^s_{xy}$ for $\widetilde{M}^s_x$ and $\theta + 3\pi/4$ for θ in Eq. (41) or (48) gives another set of the moments and forces under counter bending loading conditions. Then combining these two sets of the moments and forces gives the moments and forces of this model as

$$\widetilde{M}_r = \frac{\widetilde{M}^s_{xy}}{r^4(-1+\nu)}[(3a^4 + r^4)(1-\nu) + 4a^2r^2\nu]\sin 2\theta \tag{51a}$$

$$\widetilde{M}_{r\theta} = \frac{-\widetilde{M}^s_{xy}}{r^4}(-3a^4 + 2a^2r^2 + r^4)\cos 2\theta \tag{51b}$$

$$\widetilde{M}_\theta = \frac{\widetilde{M}^s_{xy}}{r^4(-1+\nu)}[(3a^4 + r^4)(-1+\nu) + 4a^2r^2\nu]\sin 2\theta \tag{51c}$$

$$\widetilde{Q}_r = \frac{-8\widetilde{M}^s_{xy}a^2\sin 2\theta}{r^3(-1+\nu)} \tag{51d}$$

$$\widetilde{Q}_\theta = \frac{8\widetilde{M}^s_{xy}a^2\cos 2\theta}{r^3(-1+\nu)} \tag{51e}$$

The corresponding stresses can be derived by substituting Eq. (51) into Eq. (7). By the similar argument for the case of a plate with a rigid inclusion under self-balanced counter bending moment, the moment solutions in Eq. (51) should be approximately valid for a rigid inclusion in a square plate of the width $2b$ where b/a is larger than 10. Similar operation can be used to derive the solutions for a finite square plate with a rigid inclusion using the solutions in Eqs. and (48) and (49). However, the solutions are quite complex and are not listed here.

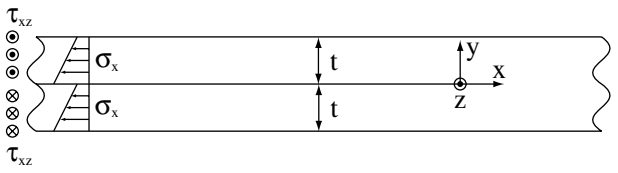

Fig. 6. A two-dimensional model of two infinite strips with connection under plane strain conditions.

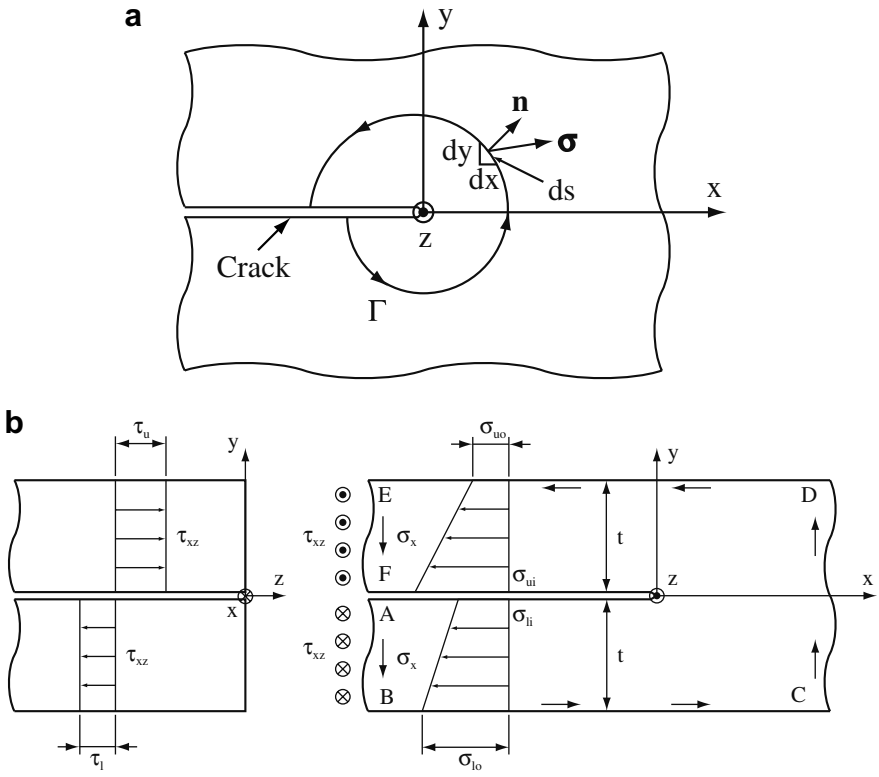

Fig. 7. (a) A crack with contour Γ surrounding a crack tip, (b) the front and side views of the left half of the strip model. The normal stresses σ_{ui}, σ_{uo}, σ_{li} and σ_{lo} represent the normal stresses σ_x at the inner (i) and outer (o) surfaces of the upper (u) and lower (l) strips, respectively. The shear stresses τ_u and τ_l represent the shear stress τ_{xz} of the upper (u) and lower (l) strips, respectively. The outside boundary line $\overline{ABCDEF}$ is considered as the contour Γ for the J integral.

6. Stress intensity factor solutions for a strip under various types of loading conditions

Once the moments, transverse shear forces and structural stresses along the rigid inclusion circumference are determined from a plate with a rigid inclusion under various types of the loading conditions, the strip model of Radaj and Zhang (1991a) can then be adopted to derive approximate stress intensity factor solutions for spot welds under various types of loading conditions. Fig. 6 shows a two-dimensional model of two infinite strips with connection under plane strain conditions. The two strips have the same thickness t. As schematically shown in Fig. 6, the radial stress σ_{rr} and the shear stress $\sigma_{r\theta}$ along the rigid inclusion circumference obtained from a plate with a rigid inclusion under various types of loading conditions are used to represent the structural stresses σ_x and τ_{xz} for the strip model, respectively, with respect to the Cartesian coordinate system as shown in Fig. 6. Note that the effects of the transverse shear stresses are neglected (Radaj, 1989; Radaj and Zhang, 1991a). The stress intensity factors can then be determined from the structural stress distributions and the J integral based on the strip model shown in Fig. 6.

For linear elastic materials, the J integral (Rice, 1968) represents the energy release rate. Under plane strain conditions, the J integral is related to K_I, K_{II} and K_{III} as

Fig. 8. Decomposition of the general structural stress distributions of a strip model. Model A represents a strip model under general distributions of the normal stresses σ_x and the shear stresses τ_{xz}. The general stress distributions of model A can be decomposed into several symmetric or anti-symmetric structural stress distributions: symmetric counter bending (model B), anti-symmetric central bending (model C), symmetric tension/compression (model D), anti-symmetric in-plane shear (model E), symmetric out-of-plane shear (model F) and anti-symmetric out-of-plane shear (model G).

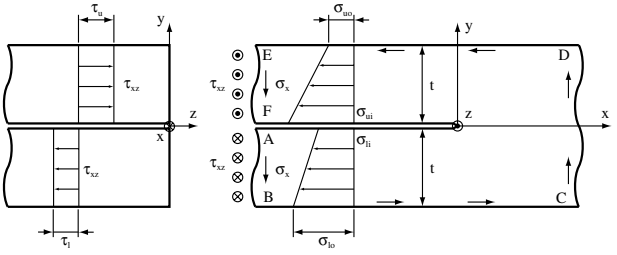

(A) (General loading)

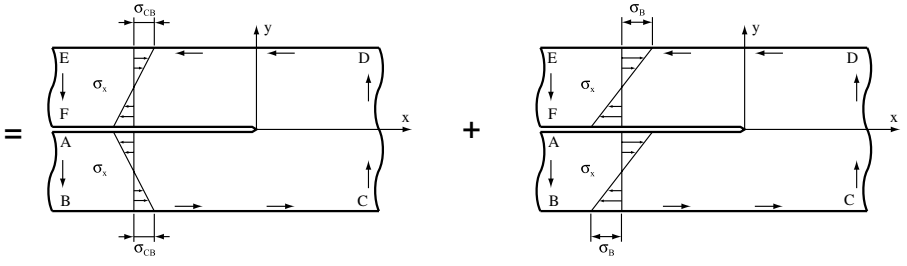

(B) (Counter bending) (C) (Central bending)

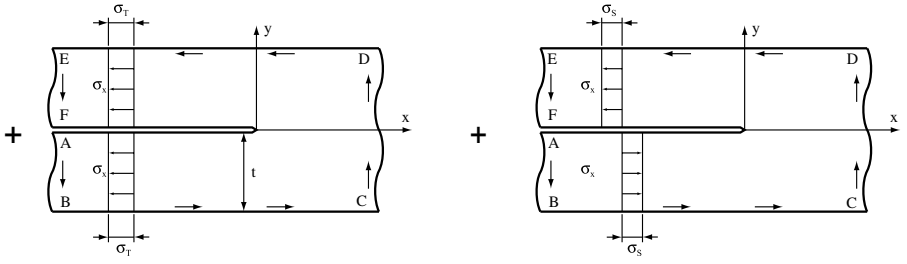

(D) (Tension/Compression) (E) (In-plane shear)

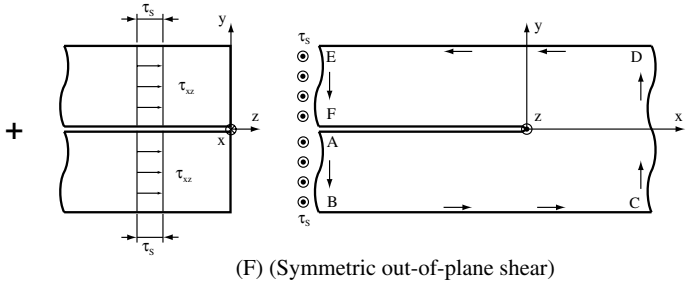

(F) (Symmetric out-of-plane shear)

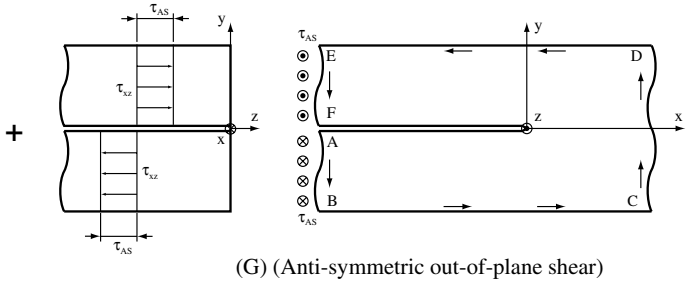

(G) (Anti-symmetric out-of-plane shear)

$$J = \frac{1-v^2}{E}(K_I^2 + K_{II}^2) + \frac{K_{III}^2}{2G} \tag{52}$$

Fig. 7(a) shows a crack and a Cartesian coordinate system centered at the crack tip. In reference to Fig. 7(a), the J integral is defined as

$$J = \int_\Gamma \left(W n_x - T_i \frac{\partial u_i}{\partial x} \right) \mathrm{d}s, i = x, y, z \tag{53}$$

where Γ represents a contour counterclockwise from the lower crack face to the upper crack face, ds represents the differential arc length of the contour Γ, n_x represents the x component of the unit outward normal **n** to the differential arc length ds, T_i ($=\sigma_{ij} n_j$) represents the components of the traction vector **T** on the differential arc length ds, and u_i represents the components of the displacement vector **u**. In Eq. (53), the strain energy density W is defined as

$$W = \int_0^{\varepsilon_{ij}} \sigma_{ij} d\varepsilon_{ij} (i, j = x,\ y,\ z) \tag{54}$$

Rice (1968) showed that the J integral is a path-independent line integral. Fig. 7(b) shows the front and side views of the left half of the strip model near the crack tip with linearly distributed structural stresses based on the classical Kirchhoff plate theory. As shown in Fig. 7(b), the normal stress σ_x and the shear stress τ_{xz} represent the structural stresses for the two infinite strips. The normal stresses σ_{ui}, σ_{uo}, σ_{li} and σ_{lo} represent the normal stresses σ_x at the inner (i) and outer (o) surfaces of the upper (u) and lower (l) strips, respectively. The shear stresses τ_u and τ_l represent the shear stress τ_{xz} of the upper (u) and lower (l) strips, respectively. Since the spot weld is modeled as a rigid inclusion with a perfect bonding to the plate, the twisting moment along the nugget circumference is zero. Therefore, τ_{xz} in the upper and lower strips are uniformly distributed through the thickness. For spot welds in various types of specimens or in automotive structural components under complex loading conditions, the deformation of the spot weld may deviate from that of a rigid inclusion. In this case, the structural stresses based on the rigid inclusion assumption may not give accurate stress intensity factor solutions along the nugget circumference (Lin and Pan, 2008b).

As shown in Fig. 7(b), the line $\overline{ABCDEF}$ is considered as the contour Γ for the J integral. The J integral is written for the contour lines $\overline{AB}$, $\overline{BC}$, $\overline{CD}$, $\overline{DE}$, and $\overline{EF}$ as

$$J = \left(\int_{\overline{AB}} + \int_{\overline{BC}} + \int_{\overline{CD}} + \int_{\overline{DE}} + \int_{\overline{EF}} \right) \left(W n_x - T_i \frac{\partial u_i}{\partial x} \right) \mathrm{d}s \tag{55}$$

where the integrals along line $\overline{BC}$ and line $\overline{DE}$ are zero because n_x is zero and T_i are zeros. For the integrals along line $\overline{AB}$, line $\overline{CD}$ and line $\overline{EF}$, the contributions of the shear stress τ_{xy} are taken to be zero in Radaj and Zhang (1991a). Recently, the three-dimensional finite element computational results of Wang et al. (2005a,b) and Lin and Pan (2008b) for various types of spot weld specimens indicate that the structural stresses from the bending moments and the membrane forces provide the dominant contributions to the stress intensity factors along the nugget circumference whereas the structural stresses from the transverse shear forces may not have significant contributions. Therefore, the J integral can be written as

$$J = -\left(\int_{\overline{AB}} W dy + \int_{\overline{CD}} W dy + \int_{\overline{EF}} W dy \right) \tag{56}$$

where the strain energy density W is

$$W = \frac{1-v^2}{2E}\sigma_x^2 + \frac{\tau_{xz}^2}{2G} \tag{57}$$

Since the integrals along line $\overline{BC}$ and line $\overline{DE}$ are zero, line $\overline{AB}$, line $\overline{CD}$ and line $\overline{EF}$ can be taken near the crack tip or at the far ends of the infinite strips by the path independence of the J integral.

Based on the works of Radaj (1989) and Radaj and Zhang (1991a), general structural stress distributions for a strip model can be decomposed into several symmetric and anti-symmetric distributions. Fig. 8 schematically shows the decomposition of the general structural stress distributions of a strip model. Schematics of

various types of structural stress distributions are shown from model A to G in Fig. 8. The general structural stress distributions are shown as model A. The structural stress distributions of model A are then decomposed into several symmetric or anti-symmetric types of structural stress distributions: symmetric counter bending (model B), anti-symmetric central bending (model C), symmetric tension/compression (model D), anti-symmetric in-plane shear (model E), symmetric out-of-plane shear (model F) and anti-symmetric out-of-plane shear (model G). The stress intensity factor K_I, K_{II} and K_{III} solutions for spot welds in various types of specimens show strong dependence on the structural stresses near the spot weld (Radaj, 1989; Radaj and Zhang, 1991a,b, 1992; Zhang, 1997, 2001). For example, the K_I solution is a function of the structural stresses near the spot weld under symmetric counter bending conditions (model B shown in Fig. 8). The K_{II} solution is a function of the structural stresses near the spot weld under anti-symmetric central bending and anti-symmetric in-plane shear conditions (models C and E shown in Fig. 8). The K_{III} solution is a function of the structural stresses near the spot weld under anti-symmetric out-of-plane shear conditions (model G shown in Fig. 8). Note that the structural stresses under symmetric tension/compression and symmetric out-of-plane shear conditions (models D and F shown in Fig. 8) have no contribution to any stress intensity factor.

The maximum values of the normal stress σ_x, marked as σ_{CB} for counter bending (model B), σ_B for central bending (model C), σ_T for tension/compression (model E) and σ_S for in-plane shear (model D), in terms of the normal stresses σ_{ui}, σ_{uo}, σ_{li}, and σ_{lo} as shown for general loading (model A) are defined as

$$\sigma_{CB} = \frac{1}{4}(\sigma_{ui} - \sigma_{uo} + \sigma_{li} - \sigma_{lo}) \tag{58a}$$

$$\sigma_B = \frac{1}{4}(\sigma_{ui} - \sigma_{uo} - \sigma_{li} + \sigma_{lo}) \tag{58b}$$

$$\sigma_T = \frac{1}{4}(\sigma_{ui} + \sigma_{uo} + \sigma_{li} + \sigma_{lo}) \tag{58c}$$

$$\sigma_S = \frac{1}{4}(\sigma_{ui} + \sigma_{uo} - \sigma_{li} - \sigma_{lo}) \tag{58d}$$

The values of the shear stress τ_{xz}, marked as τ_S for symmetric out-of-plane shear (model F) and τ_{AS} for anti-symmetric out-of-plane shear (model G), in terms of the shear stresses τ_u and τ_l as shown for general loading (model A) are defined as

$$\tau_S = \frac{1}{2}(\tau_u + \tau_l) \tag{59a}$$

$$\tau_{AS} = \frac{1}{2}(\tau_u - \tau_l) \tag{59b}$$

6.1. Solution for a strip model under counter bending (model B)

As shown in Fig. 8, model B represents a strip model under counter bending conditions. Note that the structural stresses of model B have no contribution to K_{II} and K_{III}. For model B, the integral along line $\overline{CD}$ in Eq. (56) is zero because line $\overline{CD}$ is traction free due to the self-equilibrating loading conditions of counter bending. Based on the classical Kirchhoff plate theory, the normal stress σ_x along line $\overline{AB}$ can be defined as

$$\sigma_x = \sigma_{CB}\left(1 + \frac{2y}{t}\right) \tag{60}$$

Similarly, the normal stress σ_x along line $\overline{EF}$ can be defined as

$$\sigma_x = \sigma_{CB}\left(1 - \frac{2y}{t}\right) \tag{61}$$

Combining Eqs. (56), (60) and (61) gives the J integral for model B as

$$J = \frac{-(1-\nu^2)}{2E}\left\{\int_0^{-t}\left[\sigma_{CB}\left(1+\frac{2y}{t}\right)\right]^2 dy + \int_t^0\left[\sigma_{CB}\left(1-\frac{2y}{t}\right)\right]^2 dy\right\} = \frac{\sigma_{CB}^2 t(1-\nu^2)}{3E} \tag{62}$$

Combining Eqs. (52) and (62) with $K_{II}=0$ and $K_{III}=0$ gives the K_I solution for model B as

$$K_I=\frac{\sigma_{\mathrm{CB}}\sqrt{t}}{\sqrt{3}} \tag{63}$$

6.2. Solution for a strip model under central bending (model C)

Model C represents a strip model under central bending conditions. Note that the structural stresses of model C have no contribution to K_I and K_{III}. For model C, the derivations of the integrals are similar to those for model B. However, an additional bending moment along line $\overline{CD}$ is required in order to balance the two bending moments along line $\overline{AB}$ and line $\overline{EF}$. Based on the classical Kirchhoff plate theory, the normal stress σ_x along line $\overline{AB}$ can be defined as

$$\sigma_x=-\sigma_{\mathrm{B}}\left(1+\frac{2y}{t}\right) \tag{64}$$

Similarly, the normal stress σ_x along line $\overline{CD}$ can be defined as

$$\sigma_x=\frac{-\sigma_{\mathrm{B}}y}{2t} \tag{65}$$

The normal stress σ_x along line $\overline{EF}$ can be defined as

$$\sigma_x=\sigma_{\mathrm{B}}\left(1-\frac{2y}{t}\right) \tag{66}$$

Combining Eqs. (56), (64), (65) and (66) gives the J integral for model C as

$$\begin{aligned}J&=\frac{-(1-\nu^2)}{2E}\left\{\int_0^{-t}\left[-\sigma_{\mathrm{B}}\left(1+\frac{2y}{t}\right)\right]^2\mathrm{d}y+\int_{-t}^{t}\left(\frac{-\sigma_{\mathrm{B}}y}{2t}\right)^2\mathrm{d}y+\int_t^0\left[\sigma_{\mathrm{B}}\left(1-\frac{2y}{t}\right)\right]^2\mathrm{d}y\right\}\\&=\frac{\sigma_{\mathrm{B}}^2t(1-\nu^2)}{4E}\end{aligned} \tag{67}$$

Combining Eqs. (52) and (67) with $K_I=0$ and $K_{III}=0$ gives the K_{II} solution for model C as

$$K_{II}=\frac{\sigma_{\mathrm{B}}\sqrt{t}}{2} \tag{68}$$

6.3. Solution for a strip model under in-plane shear (model E)

Model E represents a strip model under in-plane shear conditions. Note that the structural stresses of model E have no contribution to K_I and K_{III}. For model E, an additional bending moment along line $\overline{CD}$ is required in order to balance the moment due to the shear forces along line $\overline{AB}$ and line $\overline{EF}$. The detailed derivations of the integrals for the K_{II} solution are similar to those for model C and are not repeated here. The J integral for model D can be written as

$$J=-\left(\int_{\overline{AB}}W\mathrm{d}y+\int_{\overline{CD}}W\mathrm{d}y+\int_{\overline{EF}}W\mathrm{d}y\right)=\frac{\sigma_{\mathrm{S}}^2t(1-\nu^2)}{4E} \tag{69}$$

Combining Eqs. (52) and (69) with $K_I=0$ and $K_{III}=0$ gives the K_{II} solution for model D as

$$K_{II}=\frac{\sigma_{\mathrm{S}}\sqrt{t}}{2} \tag{70}$$

6.4. Solution for a strip model under anti-symmetric out-of-plane shear (model G)

Model G represents a strip model under anti-symmetric out-of-plane shear conditions. For model G, the integral along line $\overline{CD}$ in Eq. (56) is zero since $\overline{CD}$ can be considered as traction free due to the self-equilibrating anti-symmetric out-of-plane shear loading conditions. The detailed derivations of the integrals for the K_{III} solution are similar to those for model E and are not repeated here. The J integral for model G can be written as

$$J = -\left(\int_{\overline{AB}} W\mathrm{d}y + \int_{\overline{EF}} W\mathrm{d}y\right) = \frac{\tau_{\mathrm{AS}}^2 t}{G} \tag{71}$$

Combining Eqs. (52) and (71), the K_{III} solution for model G is derived as

$$K_{III} = \tau_{\mathrm{AS}}\sqrt{2t} \tag{72}$$

Note that the structural stresses for strip models under symmetric tension/compression (model D) and under symmetric out-of-plane shear (model F) have no contribution to any stress intensity factor and the J integral for them are zero.

Note that in this paper, we only focus on spot welds joining two sheets of equal thickness. In practical applications, spot welds may be used to join sheets of unequal thickness. In this case, the closed-form structural stress solutions presented in this paper remain applicable and the formulae presented in Zhang (2001) can be used to obtain the stress intensity factor solutions.

7. Conclusions

The theoretical framework and closed-form stress intensity factor solutions in terms of the structural stresses for spot welds under various types of loading conditions are presented based on elasticity theories and fracture mechanics. A mechanics description of loading conditions for a finite plate with a rigid inclusion is first presented. The loading conditions of interest are the resultant loads on the inclusion with respect to the center of the inclusion in a finite or infinite plate and the surface tractions on the lateral surface of a finite or infinite plate. The surface tractions on the lateral surface of the plate can be decomposed into a load-balanced part and a self-balanced part. The load-balanced part is statically in equilibrium with the resultant loads acting on the inclusion. The self-balanced part can be represented by the resultant loads on the lateral surface of the plate.

The resultant loads on the inclusion and the self-balanced resultant loads on the lateral surface are then decomposed into various types of symmetric and anti-symmetric parts. Based on the stress function approach and the Kirchhoff plate theory for linear elastic materials, closed-form in-plane stress, moment and transverse shear force solutions are derived for a plate with a rigid inclusion subjected to various types of resultant loads on the inclusion and various types of resultant loads on the plate lateral surface. The relevant structural stress solutions either can come from the in-plane stress solutions or can be derived easily from the moment solutions. Based on the J integral for a strip model, closed-form analytical stress intensity factor solutions for spot welds joining two sheets of equal thickness are derived in terms of the structural stresses around a rigid inclusion in a plate under various types of loading conditions. The closed-form solutions presented in this paper are used as the basis to develop new analytical stress intensity factor solutions for spot welds in various types of specimens presented in a subsequent paper (Lin and Pan, 2008a).

Acknowledgements

The support of this work from a Ford/Army IMPACT project, a Ford University Research Program, NSF grant under Grant No. DMI-0456755 at University of Michigan and a NSC grant under Grant No. 96-2221-E-194-047 at National Chung Cheng University is greatly appreciated. Helpful discussions with Dr. S. Zhang of DaimlerChrysler are greatly appreciated.

References

Goland, M., 1943. The influence of the shape and rigidity of an elastic inclusion on the transverse flexure of thin plates. Journal of Applied Mechanics 10, A-69–A-75.

Lin, P.-C., Lin, S.-H., Pan, J., 2006. Modeling of failure near spot welds in lap-shear specimens based on a plane stress rigid inclusion analysis. Engineering Fracture Mechanics 73, 2229–2249.

Lin, P.-C., Wang, D.-A., Pan, J., 2007. Mode I stress intensity factor solutions for spot welds in lap-shear specimens. International Journal of Solids and Structures 44, 1013–1037.

Lin, P.-C., Pan, J., 2008a. Closed-form structural stress and stress intensity factor solutions for spot welds in commonly used specimens. Engineering Fracture Mechanics, submitted for publication.

Lin, P.-C., Pan, J., 2008b. Three-dimensional finite element analyses of stress intensity factor solutions for spot welds in commonly used specimens, in preparation.

Michell, J.H., 1899. On the direct determination of stress in an elastic solid, with application to the theory of plates. Proceedings of the London Mathematical Society 31, 100–124.

Muskhelishvili, N.I., 1953. Some Basic Problems of the Mathematical Theory of Elasticity. Noordhoff, Groningen.

Pook, L.P., 1975. Fracture mechanics analysis of the fatigue behavior of spot welds. International Journal of Fracture 11, 173–176.

Pook, L.P., 1979. Approximate stress intensity factors obtained from simple plane bending theory. Engineering Fracture Mechanics 12, 505–522.

Radaj, D., 1989. Stress singularity, notch stress and structural stress at spot-welded joints. Engineering Fracture Mechanics 34, 495–506.

Radaj, D., Zhang, S., 1991a. Stress intensity factors for spot welds between plates of unequal thickness. Engineering Fracture Mechanics 39, 391–413.

Radaj, D., Zhang, S., 1991b. Simplified formulae for stress intensity factors of spot welds. Engineering Fracture Mechanics 40, 233–236.

Radaj, D., Zhang, S., 1992. Stress intensity factors for spot welds between plates of dissimilar materials. Engineering Fracture Mechanics 42, 407–426.

Rice, J.R., 1968. A path independent integral and the approximate analysis of strain concentration by notches and cracks. Journal of Applied Mechanics 35, 379–386.

Reißner, H., 1929. Über die unsymmetrische biegung dünner kreisringplatten. Ingenieur-Archiv 1, 72–83.

Rupp, A., Grubisic, V., Radaj, D., 1990. Betriebsfestigkeit von Punktschweissverbindunghen. Sonderdruck aus Materialprüfung 32, 1–6.

Rupp, A., Storzel, K., Grubisic, V., 1995. Computer aided dimensioning of spot welded automotive structures. SAE Technical Paper No. 950711. Society of Automotive Engineers, Warrendale, PA.

Salvini, P., Scardecchia, E., Vivio, F., 1997. Fatigue life prediction on complex spot weld joints. SAE Transaction, Journal of Materials and Manufacturing 106, 967–975.

Salvini, P., Vivio, F., Vullo, V., 2000. A spot weld finite element for structural modeling. International Journal of Fatigue 22, 645–656.

Salvini, P., Vivio, F., Vullo, V., 2007. Extension of the spot weld element to the elastic-plastic case. SAE Technical Paper No. 2007-01-1361, Society of Automotive Engineers, Warrendale, PA.

Sheppard, S.D., 1993. Estimation of fatigue propagation life in resistance spot welds. In: Mitchell, M.R., Landgraf, R.W. (Eds.), Advances in Fatigue Lifetime Predictive Techniques, . In: ASTM STP 1211, vol. 2. American Society for Testing and Materials, Philadelphia, pp. 169–185.

Swellam, M.H., Banas, G., Lawrence, F.V., 1994. A fatigue design parameter for spot welds. Fatigue and Fracture of Engineering Materials and Structures 17, 1197–1204.

Timoshenko, S., Woinowsky-Krieger, S., 1959. Theory of Plates and Shells, second ed. McGrow-Hill, New York.

Vivio, F., Ferrari, G., Salvini, P., Vullo, V., 2002. Enforcing of an analytical solution of spot welds into finite element analysis for fatigue-life estimation. International Journal of Computer Applications in Technology 15, 218–229.

Wang, D.-A., Lin, S.-H., Pan, J., 2005a. Stress intensity factors for spot welds and associated kinked cracks in cup specimens. International Journal of Fatigue 27, 581–598.

Wang, D.-A., Lin, P.-C., Pan, J., 2005b. Geometric functions of stress intensity factor solutions for spot welds in lap-shear specimens. International Journal of Solids and Structures 42, 6299–6318.

Young, W.C., Budynas, R.G., 2002. Roark's Formulas for Stress and Strain. McGraw-Hill, New York.

Zhang, S., 1997. Stress intensities at spot welds. International Journal of Fracture 88, 167–185.

Zhang, S., 1999. Approximate stress intensity factors and notch stress for common spot-welded specimens. Welding Research Supplement 78, 173s–179s.

Zhang, S., 2001. Fracture mechanics solutions to spot welds. International Journal of Fracture 112, 247–274.